

# Polymer Chemistry

Accepted Manuscript



This is an *Accepted Manuscript*, which has been through the Royal Society of Chemistry peer review process and has been accepted for publication.

*Accepted Manuscripts* are published online shortly after acceptance, before technical editing, formatting and proof reading. Using this free service, authors can make their results available to the community, in citable form, before we publish the edited article. We will replace this *Accepted Manuscript* with the edited and formatted *Advance Article* as soon as it is available.

You can find more information about *Accepted Manuscripts* in the [Information for Authors](#).

Please note that technical editing may introduce minor changes to the text and/or graphics, which may alter content. The journal's standard [Terms & Conditions](#) and the [Ethical guidelines](#) still apply. In no event shall the Royal Society of Chemistry be held responsible for any errors or omissions in this *Accepted Manuscript* or any consequences arising from the use of any information it contains.

## ARTICLE

# Highly homogeneous core-sheath polyaniline nanofibers by polymerisation on wire-shaped template

Cite this: DOI: 10.1039/x0xx00000x

Received 00th January 2012,  
Accepted 00th January 2012

DOI: 10.1039/x0xx00000x

www.rsc.org/

Rossella Castagna<sup>a</sup>, Roberto Momentè<sup>a</sup>, Giorgio Pariani<sup>b</sup>, Giuseppe Zerbi<sup>a</sup>,  
Andrea Bianco<sup>b</sup>, Chiara Bertarelli<sup>a,c\*</sup>

Defect-free and highly homogeneous Polyaniline (PANI)–Nylon 6 electrospun nanofibers are obtained through a solvent-induced segregation of N-phenyl-1,4-phenylenediamine (ADPA) on the fiber surface followed by an oxidative surface polymerization onto the wire-shaped template. Different oxidation salts are tested both as additives of the spinning solutions and in the polymerization bath. Comparison between mats obtained with solvent induced segregation process and classical feed solution electrospinning is highlighted. As a result, self-standing emeraldine base PANI (EB) membranes are produced both in this pristine state and in a doped emeraldine salt state (ES). Doping process is carried out in different acid baths, namely hydrochloric acid, sulfuric acid and p-toluene sulphonic acid, the last being the most effective. Wire-shaped PANI membranes are characterized by scanning electron microscopy (SEM) and the polymerization/doping states of PANI are monitored step by step by UV-vis reflectance spectroscopy, infrared spectroscopy (FTIR), and contact angle measurements (CA).

## Introduction

One-dimensional nanomaterials, in particular nanofibers and nanofibrous nonwovens, are unique nanostructures with extraordinary potential in technological context<sup>1</sup> and in medical application<sup>2,3</sup>. Filtering,<sup>4,5</sup> functionalization of textiles<sup>6</sup>, fiber reinforcement<sup>7,8</sup>, catalysis<sup>9</sup>, drug delivery<sup>10</sup>, wound healing<sup>11,12</sup> or tissue engineering<sup>13,14</sup> are just some examples of new opportunities. Among the different technologies<sup>15,16</sup> to afford nanorods, nanowires or nanofibers, electrospinning is the only one which enables the fabrication of continuous polymer fibers with diameters down to a few nanometers<sup>17–19</sup>. The high surface to volume ratio of nanofibers, which improves the material sensitivity as respect to the bulk, combined with a relative large productivity, make electrospun nanofibers very attractive for sensing<sup>20,21</sup>. In electrospun materials, chemical sensing<sup>22,23</sup> has been demonstrated when intrinsic conducting polymers (ICP), such as polyaniline (PANI), are employed<sup>24</sup>. The interest towards PANI comes from its versatile synthesis<sup>25,26</sup> and doping chemistry<sup>27,28</sup>, high conductivity<sup>29,30</sup> and excellent environmental stability<sup>31</sup>. Moreover, in contrast to classical metallic conductors or polymeric insulators, PANI can be reversibly switched by protonation and deprotonation between a semiconductive emeraldine base form and a conductive emeraldine salt<sup>32–34</sup>. Different composites with gold<sup>35</sup> or silver<sup>36</sup> nanoparticles embedded to PANI polymer are recently reported. Furthermore PANI/composite systems were proposed as active filters of hazardous elements in water, such as mercury<sup>37,38</sup> and chromium (VI)<sup>39,40</sup>. Unfortunately, processing to produce PANI fibers is not straightforward. To overcome this issue, several

approaches have been reported<sup>41</sup>. One strategy include blending PANI with a polymer which supports the fiber formation<sup>42–45</sup>. However, the presence of this insulating component often prevents high electrical conductivities to be achieved. Although the supporting material can be removed by a selective rinsing<sup>46</sup>, the fibrous morphology can be strongly affected by this post-processing. Core-sheath PANI fibers with excellent morphology and remarkable conductivity have been demonstrated by means of coaxial electrospinning<sup>47–49</sup> that, however, requires a very fine process optimization to have a control over the process.

Another interesting method to obtain core-sheath nanofibers with an outer conductive polymer consists in the production of a polymer mat to act as a template and the subsequent *in situ* polymerization of monomers to form a sheath of an intrinsically conducting polymer grown onto the template<sup>50,51</sup>. This approach has been employed in the case of polypyrrole<sup>52,53</sup> and also of PANI, with the polymerization of the latter being performed in solution with a two-step process, namely the diffusion of the monomer onto the fibers surface followed by the oxidative polymerization of the adsorbed monomer by addition of ammonium persulfate in an acidic medium<sup>21,47,50</sup>. As a matter of fact, the process leads to rough fiber surfaces and not uniform fiber mats. Moreover, PANI particles deposition often occurs not only onto the fiber template but also between fibers and randomly in the mat, which turns into a poor quality of the final coating.

In this paper we demonstrate the production of emeraldine salt (ES) defect-free PANI nanofibers produced through a novel and simple approach. The polymer membrane is prepared by the

spontaneous segregation of *N*-phenyl-1,4-phenylenediamine (ADPA) onto Nylon 6 fiber surface during the electrospinning and the subsequent polymerization of this template upon immersion into a solution containing an oxidant agent and an acidic species. A doping process leads to PANI fibers in the ES form. The presence of the aniline dimer only on the template surface drives the formation of a homogenous PANI sheath on the fiber template, disabling any polymerization out of the fibers. As a result, PANI self-standing membranes with exceptionally uniform and smooth fiber morphology are attained.

## Experimental method

**Materials** Nylon 6 in pellets, formic acid (puriss. p.a., ~98%), iron(III) chloride anhydrous ( $\text{FeCl}_3$ ), iron(III) hexahydrate ( $\text{FeCl}_3 \cdot 6\text{H}_2\text{O}$ ), *N*-phenyl-*p*-phenylenediamine 98% (ADPA), ammonium persulfate (APS, 98%), acetone ( $\geq 99.5\%$ ), oxalic acid ( $\geq 99\%$ ), hydrochloric acid (37%) and *p*-toluenesulfonic acid monohydrate (p-TSA,  $\geq 98.5\%$ ) were purchased from Sigma Aldrich. All reagents were used as received.

### Preparation of the feed solutions

***N-FeA*** - Nylon 6 and  $\text{FeCl}_3$  anhydrous: Nylon 6 pellets (15 wt% with respect to formic acid) were dissolved in formic acid, then anhydrous iron chloride (5.6 wt% with respect to formic acid) was added..

***N-FeH*** - Nylon 6 and  $\text{FeCl}_3 \cdot 6\text{H}_2\text{O}$ : Nylon 6 pellets (15 wt% with respect to formic acid) were dissolved in formic acid, then hexahydrate iron chloride (8.85 wt% with respect to formic acid) was added..

***N-sFeH*** - Nylon 6 and segregated  $\text{FeCl}_3 \cdot 6\text{H}_2\text{O}$ : Nylon 6 pellets and hexahydrate iron chloride were separately dissolved in formic acid and acetone, respectively. Nylon 6 concentration was set at 25 wt% (with respect to formic acid), while  $\text{FeCl}_3 \cdot 6\text{H}_2\text{O}$  concentration was 8.85 wt% (with respect to Nylon 6). Acetone and formic acid were taken in ratio 2:7 (v/v). Once total dissolutions were reached, the two solutions were mixed and the mixture was magnetically stirred until a homogeneous phase was obtained.

***N-sADPA*** - Nylon 6 and segregated *N*-phenyl-1,4-phenylenediamine (ADPA): Nylon 6 pellets were dissolved in formic acid, while separately ADPA was dissolved in acetone. Nylon 6 concentration was set at 25 wt% (with respect to formic acid), while different concentrations of ADPA were considered (48, 54, 60.5, 67, 73 wt% with respect to Nylon 6). Acetone and formic acid were taken in ratio 2:7 (v/v). Once total dissolution was reached, the two solutions were mixed and the mixture was magnetically stirred until a homogeneous phase was obtained.

***N-ADPA*** - Nylon 6 and *N*-phenyl-1,4-phenylenediamine (ADPA): formic acid solutions of Nylon 6 (25 wt% with respect to formic acid) containing ADPA (67 wt% with respect to Nylon 6) were prepared..

***N6*** - Nylon 6: formic acid solutions of Nylon 6 (25 wt% with respect to formic acid) with no other additives were prepared.

**Polymer Fibers by Electrospinning** Electrospinning was performed by loading the polymer solution in a 2,5 mL syringe with a 22 gauge needle (Hamilton Gastight model 1002 TLL), which was then mounted on a infusion pump (KDS Scientific, model series 200) that feeds the solution into the capillary nozzle at a constant flow rate of 0.05 ml/h. All the electrospinning runs were carried out at room temperature using a bottom-up vertical configuration. Voltage was applied to the needle by a High Voltage Power Supply (Spellman SL30P300). Fibers were collected randomly on glass and on silicon substrates; the best setup parameters are listed in table 1.

Preparation	Voltage (kV)	Tip-collector distance (cm)	Flow rate (ml/h)
N-FeA	15	20	0.05
N-FeH	15	20	0.05
N-sFeH	20	10	0.05
N-sADPA	17	10	0.05
N-ADPA	18	20	0.05
N6	18	20	0.05

**Table 1.** Electrospinning parameters of the preparation sets.

**Diffusion step** A diffusion bath containing an aqueous solution of *N*-phenyl-1,4-phenylenediamine (0.125 M) and HCl (0.175 M) was prepared and heated at 40°C until the complete dissolution. The N-FeH and N-sFeH electrospun fiber webs collected on a glass or silicon substrates, were immersed in the solution. Samples were then rinsed in acetone and distilled water, then dried with filter paper and stored under hood for one night to ensure a gentle and complete drying.

**Oxidative polymerization** Polymerization was performed by immersing the samples i) after diffusion step for N-sFeH set or ii) as spun for N-sADPA set in an oxidation bath containing APS (0.125 M) and HCl (0.175 M) at 0°C. The effect of other acids, such as oxalic acid and *p*-toluenesulfonic acid (p-TSA) keeping constant the molar concentration was also tested. This step was carried out in ice bath<sup>21,45</sup> in order to slow down the reaction kinetics and have a better control over the polymerization rate. For N-sFeH set oxidation time was set at 30 min. Conversely, different oxidation times were tested for N-sADPA as this procedure has never been investigated so far. The core/sheath fiber webs were then washed with distilled water, dried with filter paper and stored under hood until the complete evaporation of the solvent..

**Doping.** Doping was carried out upon immersion of the samples in an acidic solution, followed by drying with filter paper to remove the excess of acid. Different acids, including HCl, oxalic acid ( $\text{H}_2\text{C}_2\text{O}_4$ ), sulfuric acid ( $\text{H}_2\text{SO}_4$ ) and *p*-toluenesulfonic acid ( $\text{CH}_3\text{C}_6\text{H}_4\text{SO}_3\text{H}$ ) were tested at different concentrations, namely 1 M, 0.5 M and 0.175 M.

**Characterization** A high resolution Scanning Electron Microscope (SEM), FEG LEO 1525 was used to collect electron micrographs of the electrospun fibers. No conductive coating was deposited onto the samples. The mean diameter and distribution from the SEM images were determined with ImageJ software (Rasband, W.S., ImageJ, U. S. National Institutes of Health, Bethesda, Maryland, USA,

<http://rsb.info.nih.gov/ij/>, 1997–2008). Contact angles (CA) were measured with an OCA system-DataPhysiscs according to the sessile method. Fourier transform infrared spectroscopy (FT-IR) was performed in transmission mode by using a Nicolet NEXUS FTIR interferometer (DTGS detector) on free-standing electrospun membranes. The ADPA spectrum was collected from a drop cast film from acetone on ZnSe substrate. The resolution was  $0.1\text{ cm}^{-1}$  and 256 sample scans were acquired. Omnic 7.1 software (Thermo Nicolet Instrumentation) was used to analyze the spectra. Ultraviolet-visible (UV-vis) absorption spectra were recorded on a Varian Cary 5000 spectrophotometer with the integrating sphere to measure the diffuse reflectance of the fiber mats.

## Results and discussion

The electrospinning of conjugated polymers is generally rather demanding because of their limited solubility, relatively low molecular weight and rigid backbone. Among the possible methods reported in literature to produce conjugated polymer fibers<sup>54–56</sup>, we referred to polymerization onto fiber template, which allows the production of fibers with an insulating core and a conducting sheath. We have previously demonstrated that exposing an electrospun polymer template containing an oxidizing salt to pyrrole vapours a polymerization occurs at the fibers surface to afford Nylon 6/polypyrrole fibers<sup>53</sup>.

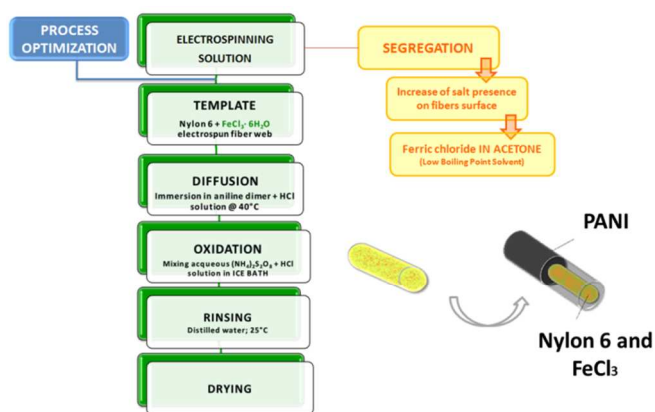
Herein we applied a similar procedure to produce polyaniline (PANI) fibers. Nylon 6 was chosen as core polymer since it has been widely electrospun and the stability of polyamide to many solvents makes it suitable for a wide range of applications. Literature reports ammonium persulfate (APS) as the common oxidant employed in PANI synthesis<sup>29</sup>. However, APS cannot be directly dissolved in the Nylon 6 feed solution since formic acid reduces it to sulfate, disabling its ability to polymerize aniline. For this reason, iron (III) was used. If compared with APS, iron (III) chloride is characterized by a lower oxidation potential, which is not high enough to promote the aniline polymerization. Interestingly, this problem can be overcome if, instead of aniline, *N*-phenyl-*p*-phenylenediamine ADPA is used as starting monomer<sup>29</sup>.

Hexahydrate iron (III) chloride was preferred to the anhydrous one as the latter is highly hygroscopic. A good fiber morphology was obtained by using the same molar amount of anhydrous salt which has been tested in a previous work<sup>53</sup> (See ESI Figure 1). However, during the following polymerization steps, consisting in the monomer diffusion and oxidation in acidic medium, polyaniline growth suffered from poor control (See ESI Figure 2). We have tentatively ascribed this fact to the lack of a sufficient quantity of iron chloride onto the fiber surface to promote a uniform PANI polymerization. Acetone was added to the formic acid to promote segregation of the  $\text{FeCl}_3 \cdot 6\text{H}_2\text{O}$  during the flight of the spun jet<sup>57</sup>. Surface segregation was expected to improve the polymerization efficiency, the quantity of salt available onto the template surface being larger. The experimental flow chart of this strategy is shown in Scheme 1.

Acetone was chosen for the solvent induced segregation since it i) easily dissolves hexahydrate iron (III) chloride, ii) shows a boiling point ( $56^\circ\text{C}$ ) lower than formic acid ( $100.8^\circ\text{C}$ ), so it evaporates faster than the main solvent and iii) it is a bad solvent for polyamides.

The volume ratio between acetone and formic acid was optimized from 0:1 v/v to 3:7 v/v in order to dissolve the maximum quantity of  $\text{FeCl}_3 \cdot 6\text{H}_2\text{O}$ , while avoiding instability. The best condition was 2:7 v/v of acetone to formic acid ratio

with 8.85 wt% of  $\text{FeCl}_3 \cdot 6\text{H}_2\text{O}$  with respect to Nylon 6 (25 wt% with respect to formic acid).



**Scheme 1.** Flow chart of the process to yield N-sFeH fibers. On the right: the sketch of the resulting core-sheath fiber mat.

The SEM analysis (see Figure 1a) showed defect-free electrospun fibers with a mean diameter of  $217 \pm 40\text{ nm}$ .

The presence of segregated iron nanostructures cannot be highlighted by SEM due to the very thin nanofiber diameters. In the literature Nylon 6 is electrospun from hexafluoroisopropanol<sup>58</sup> to give fibers with larger diameters thus allowing to investigate details of the fiber surface. However,  $\text{FeCl}_3 \cdot 6\text{H}_2\text{O}$  is not soluble in hexafluoroisopropanol.

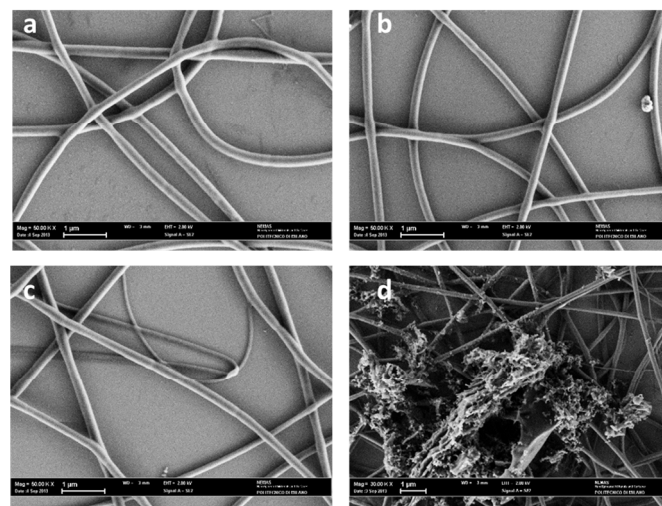


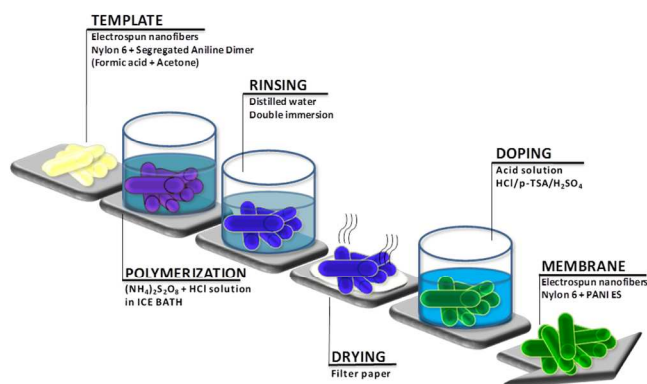
**Figure 1.** Morphological characterization of N-sFeH (8.85 wt%  $\text{FeCl}_3 \cdot 6\text{H}_2\text{O}$ ) electrospun nanofibers: a) SEM image at 20 kV, flow rate of 0.05 mL/h and tip-collector distance of 10 cm. SEM images of N-sFeH electrospun nanofibers after a diffusion step of b) 180' and c) 120' d) SEM images of N-sFeH electrospun nanofibers  $t_{\text{DIFF}} = 180' + t_{\text{OX}} = 30'$ .

Immersion in an acidic aqueous solution of APDA for 120 and 180 minutes ( $t_{\text{diff}}$ ), to promote diffusion of the aniline dimer onto the fiber surface and its possible polymerization, did not affect fiber morphology and size. Statistical analysis of mean diameters for N-sFeH fibers at different diffusion times shows

no significant changes of fiber diameter and morphology, as reported in Figure 1b-c and ESI figure 9.

This result leads to the hypothesis that no polymerization occurred onto the fiber surface. Fibers were then immersed in an oxidation bath to further promote polymerization, but just new rough aggregates covered the fibrous mat (Figure 1d oxidation time 30' ( $t_{ox}$ )). Despite fibers are expected to be likely coated by PANI, the presence of these large defective islands suggests a poor control over the polymerization and a low template induced-effect ruled by the Nylon/FeCl<sub>3</sub> mat.

**Nylon 6 and segregated N-phenyl-1,4-phenylenediamine (ADPA) template nanofibers** As PANI did not uniformly coat fibers or, in the last case, no uniform control over the template polymerization was achieved, any procedure involving the addition of oxidant salts in the Nylon fiber template has not been further considered. Alternatively, the feed solution was loaded with the aniline dimer instead of the oxidant and segregation was solvent-induced to maximize the dimer concentration at the surface. Afterwards, the fibrous template with the surface-segregated ADPA was polymerized upon immersion in the oxidation bath (Scheme 2). This procedure lowers the number of steps as the polymerization occurs in a single reaction bath containing both the oxidant salt and the acidic species without any diffusion step of the aniline monomer or dimer.



**Scheme 2.** Flow chart of the experimental process carried out on Nylon 6 and segregated ADPA blend.

**Template production** Different solutions of Nylon 6 (25 wt% with respect to formic acid) and ADPA in formic acid and acetone (ratio 2:7 (v/v) with respect to formic acid) were electrospun in order to determine the maximum loading concentration of ADPA (from 0 wt% to 73 wt% with respect to Nylon 6) to guarantee a stable electrospinning process. SEM images of the electrospun mats collected starting from different aniline dimer concentrations are reported in Figure 2. Despite defect free fibers were obtained at every condition, electrospinning underwent instability when aniline dimer concentration was increased to 73 wt.

Interestingly, no segregated spot onto the fibers surface is evident, thus leading to the hypothesis that a uniform segregation at the fiber surface occurred. Electrospun nanofibers containing 67 wt% of ADPA (Figure 2e) were considered for the following study.

To highlight the effect of ADPA segregation onto the fiber surface, analogous non-segregated N-ADPA mats were prepared, resulting in good fiber morphology also in this case (see ESI Figure 3).

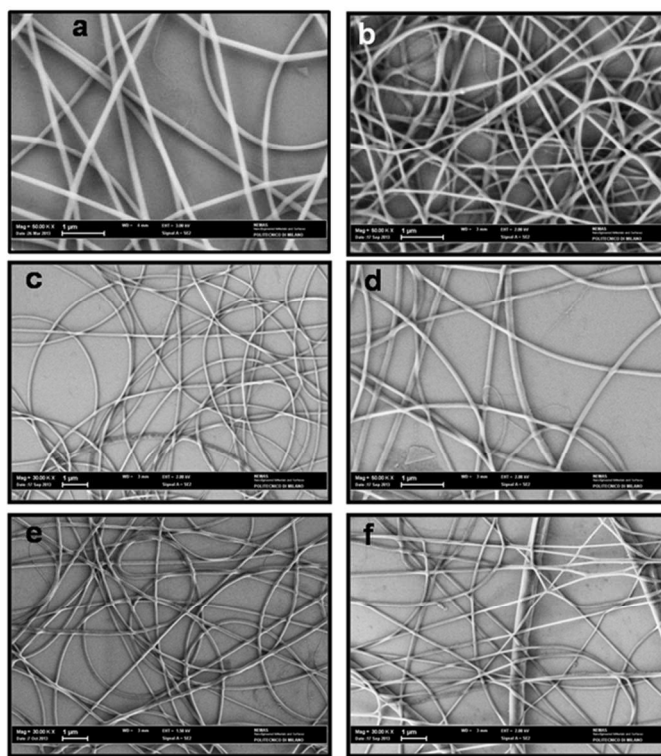


**Figure 2.** SEM images of N-sADPA loaded with different ADPA concentrations: a) 0% b) 48% c) 54%; d) 60.5%; e) 67%; f) 73% wt% ADPA with respect to Nylon 6.

Surface segregation of the aniline dimer during the fiber formation was monitored by contact angles (CA) measurements: a contact angle value of 122° was obtained for the pure Nylon 6 fiber mat, which is well consistent with that reported by Pant *et al.*<sup>59</sup>. By addition of aniline dimer into the feed solution, CA reduces till reaching a *plateau* at concentration higher than 60 wt% (Figure 3). Decreasing of contact angle while increasing surface segregation is related to the presence of amine groups in the N-phenyl-p-phenylenediamine.

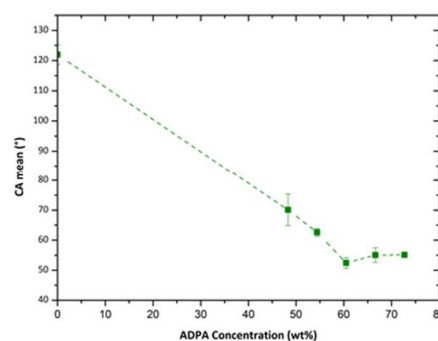


**Figure 3.** Contact angle of Nylon 6 and N-sADPA electrospun nanofibers with different ADPA concentration.

UV-Vis spectra in diffuse reflectance were recorded on both fiber samples prepared with and without the presence of acetone in the feed solution. Figure 4 reports the values 1-R (magnification of visible region is reported in the ESI Figure 4).

The curve of the pure Nylon 6 mat (green line) shows the typical trend of a scattering material with no absorption in all the region 250-2500 nm.

On the contrary, the absorption fingerprints at 290, 420 and 625 nm typical of ADPA are evident in N-sADPA and N-ADPA<sup>60</sup>.

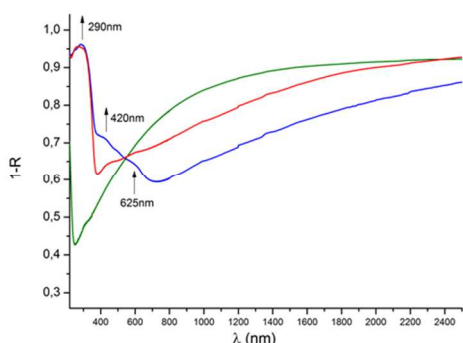


**Figure 4.** UV-Vis diffuse reflectance spectra of Nylon 6 fiber mats (green line), N-sADPA (blue line) and N-ADPA (red line).

However, the relative intensity of these features differs between the segregated and non-segregated samples, the former being characterized by a higher absorption in the regions corresponding to the ADPA bands. This evidence demonstrates that the presence of acetone in the feed solution is effective in ADPA segregation at the fibers surface.

Relevant information on the interaction between polyamide and the aniline dimer was obtained from FTIR spectroscopy (figure 5). The detailed peak assignment of the two components is reported in Table 1 of the ESI. It is worth noting that the bands associated to amide I and amide II vibrations (at 1650 and 1542  $\text{cm}^{-1}$ , respectively) of the pure Nylon 6 mat are broad, being affected by all the possible conformations of the methylene segments. When Nylon 6 is loaded with ADPA, a significant sharpening of the amide I and II peaks is noted, which leads to the hypothesis that an interaction between the aniline dimer and nylon amide groups actually occurs that hampers some possible conformations in the polyamide chain. This hypothesis is further confirmed by the weakening of the N-H stretching of the aniline dimer (See ESI Fig 5).

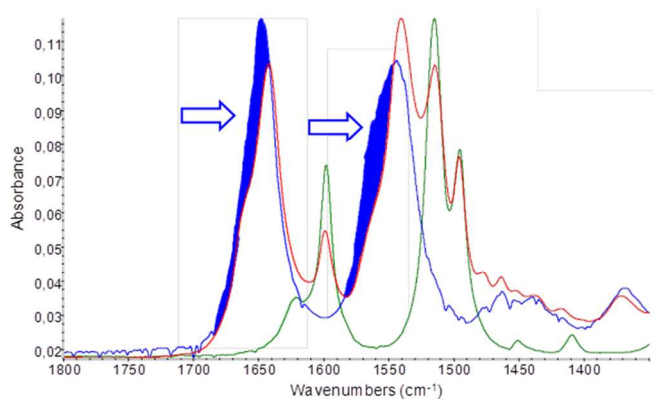


**Figure 5.** FTIR spectra of electrospun N6 (blue line) and N-sADPA mats (red line), and ADPA film (green line). Narrowing of the amide I and amide II is highlighted in blue.

Polymerization does not affect either the fibrous morphology and fibers size distribution (figure 6 and ESI figure 10). By statistical analysis of the electrospun mats it turns out that the mean fiber diameter was equal to  $160 \pm 30 \text{ nm}$  before polymerization and  $150 \pm 30 \text{ nm}$  after oxidative polymerization. Therefore, the final PANI mat has a similar diameter distribution of the Nylon 6 template. Acting on the solution parameters, such as polymer concentration, and processing conditions as voltage and flow rate it is possible to control the fiber diameter of the final mat.

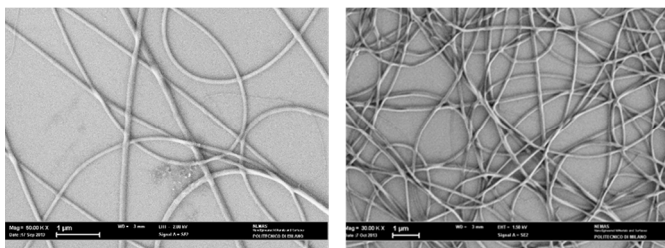


**Figure 6.** N-sADPA (ADPA 67 wt% with respect to Nylon 6) On the left: SEM image after oxidative polymerization ( $t_{\text{ox}} = 150 \text{ s}$ ); On the right: after doping in HCl (0.175 M).

**Oxidative polymerization** Upon immersion of N-sADPA (67 wt% ADPA/Nylon6) in the oxidation bath, polymerization occurred at the fibers surface. Oxidation bath temperature was set to  $0^\circ\text{C}$  since at room temperature the polymerization kinetics is too fast.

Immersion in the oxidative bath was varied from 30 s, 150 s, 300 s, 450 s to 600 s to determine the best time scale for polymerization to get complete while avoiding an overoxidation of the PANI<sup>29</sup>.

During polymerization by immersion in APS (0.125 M) and HCl (0.175 M) bath the ivory fibrous membrane turned dark grey while right after the immersion, then pale blue. After rinsing in water and drying, the final color of the mat was bluish, typical of emeraldine base (figure 7).

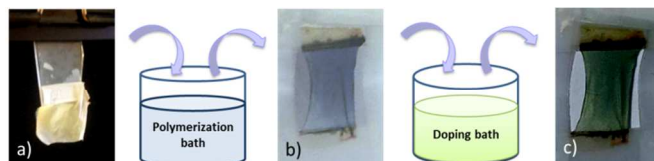


**Figure 7.** Colour turning of the N-sADPA electrospun nanofibrous membrane after oxidative polymerization and doping steps: a) free-standing fibrous membrane as spun; b) after oxidative polymerization step:  $t_{\text{ox}} = 150 \text{ s}$  in APS (0.125 M) and HCl (0.175 M); c) after the following doping step:  $t_{\text{dop}} = 30 \text{ s}$  in HCl (0.175 M).

The effects of other acids, such as oxalic acid or p-toluenesulfonic acid (p-TSA), were tested (0.175 M). The former showed poor solubility at the polymerization conditions, whereas fibers were successfully polymerized with p-TSA. Despite fibrous morphology was retained after oxidation, SEM images showed the presence of some shining spots, probably associated to residual p-TSA (See ESI Figure 6).

The formation of PANI onto the fibers surface upon immersion of the mat in the oxidation bath containing APS (0.125 M) and HCl (0.175 M) was monitored by contact angle measurements UV-Vis and infrared spectroscopy.

The CA value of the electrospun mat increases after polymerization (see figure 8), as the primary amine groups of ADPA, react during the oxidation step.

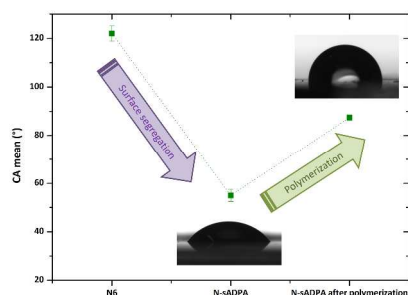


**Figure 8.** Contact angle (CA) measurements of N6 nanofiber mat, as-spun N-sADPA mat, N-sADPA mat after oxidation in APS (0.125 M) for 150 s. Each value arises from the average of at least ten measurements on different points of the same sample.

UV-Vis spectra collected in diffuse reflectance mode, of samples after 20, 50 and 120 seconds of immersion in the polymerization bath were recorded. Relative spectra obtained as the ratio  $R$  (as spun)/ $R$  (ox) to avoid the scattering issue and highlight the differences are reported in figure 9 (as recorded spectra is reported in ESI Figure 7).

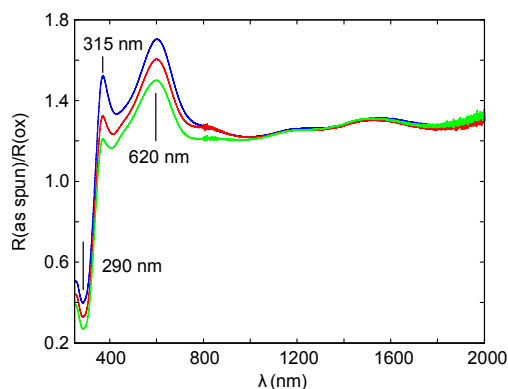


**Figure 9.** UV-Vis reflectance spectra of N-sADPA (67 wt% ADPA vs Nylon 6) electrospun nanofibers  $t_{ox} = 20$  s (blue);  $t_{ox} = 50$  s (red);  $t_{ox} = 120$  s (green).  $R(\text{as spun}) / R(\text{ox})$  spectra.

The growth of absorption bands at 315 nm and at 620 nm is consistent with the electronic transitions in emeraldine base<sup>61,62</sup>, as sketched in fig. 10, while the decrease in absorption at 290 nm indicates that the ADPA was exhausted during polymerization<sup>63,64</sup>.

Although UV-Vis reflectance spectroscopy clearly demonstrates polymerization to occur, the kinetics of the process could not be quantitatively determined as spectra suffer from the scattering due to the fibrous morphology, and a common baseline could not be set.

It is known that doping leads to the formation of charged species (e.g. polarons and bipolarons), which are evidenced by the appearance of a broad electronic band at longer wavelengths in the UV-vis spectra. As regards PANI, the position of the polaronic absorption bands shifts to a longer wavelength while increasing the size of the dopant. Specifically, PANI doped with a smaller dopant shows a polaronic band located at 800–900 nm, whereas a band above 1000 nm characterizes PANI doped with a larger dopant<sup>29,65</sup>.

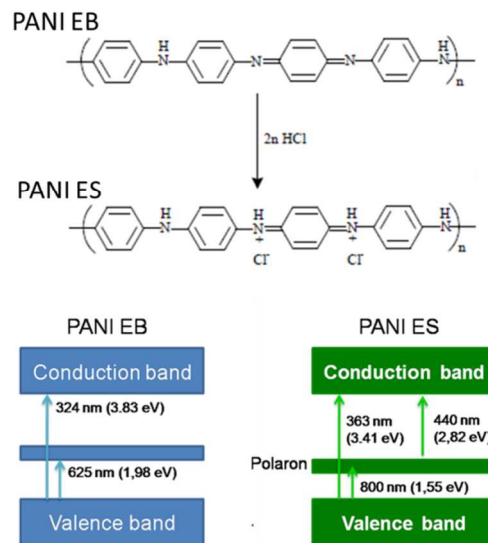


**Figure 10.** Energy diagrams and molecular structure of PANI before doping (emeraldine base form EB) and after doping with HCl (emeraldine salt ES) (values of level transitions adapted from the literature<sup>66</sup>).

Conversely, it is possible to monitor the reaction proceeding by IR spectroscopy, following some vibrational modes which are strongly modified during the PANI formation (Figure 11).

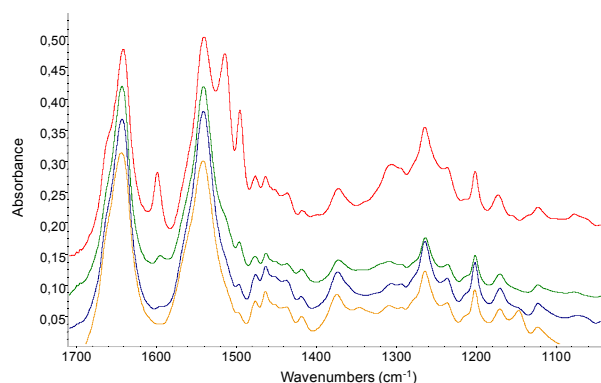


**Figure 11.** FTIR spectra of N-sADPA (67 wt% ADPA vs Nylon 6) in wavenumbers range 1700 - 500  $\text{cm}^{-1}$  at different oxidation times: before oxidation step (red);  $t_{ox} = 10$  s (green);  $t_{ox} = 30$  s (blue);  $t_{ox} = 150$  s (orange).

A gradual disappearing of the peaks near 1600  $\text{cm}^{-1}$  occurs, which are fingerprints of the aniline dimer. These features are associated to the aromatic ring stretching and to the N-H bending of the primary amine ( $-\text{NH}_2$ ), which is the functional group involved in the polymerization reaction. This band totally disappears after 150 s of polymerization, so this time was adopted as the optimal to complete the polymerization.

For prolonged oxidation time ( $t_{ox} = 150$  s), a band at 1147  $\text{cm}^{-1}$  is observed, that has been assigned according to ref<sup>67</sup>, to the vibrations of the positive charged polymer units  $\text{Q}=\text{NH}^+-\text{B}$  or  $\text{B}-\text{NH}^+-\text{B}$ , where Q indicates quinoid structure while B the benzenoid one. It means that a slight protonation may

accompany oxidation, which is reasonable since polymerization occurs in an acidic environment. Although this assignment could be object of criticism since many vibrations lie in this frequency range, this hypothesis has also been confirmed by the spectra collected after a base treatment (see ESI figure 11 on the right), which was carried out upon immersion the sample in an aqueous solution of KOH (0.175 M). Band at  $1147\text{ cm}^{-1}$  completely disappears, thus indicating that alkaline treatment has effectively removed the partial doping.

**Doping step** In order to convert polyaniline from the blue emeraldine base form to the conductive green emeraldine salt, a doping process was carried out in an acidic environment. 1 M and 0.5 M HCl resulted too aggressive and a damage of the fabric was observed. Immersion into 0.175 M HCl doping bath, which is the same concentration used in the polymerization, did not affect the homogeneity and uniformity of the mat (see figure 6 on the right). To avoid possible damaging of the fibers, the excess of acid was removed by drying the fibrous mat onto an absorbing paper. Doping time was set at 30 s. The statistical analysis on the diameters evidenced that the distribution frequency, with average diameter of  $140 \pm 20\text{ nm}$ , did not change by doping (see ESI fig. 10). Doping was also performed with oxalic acid, p-TSA and sulfuric acid and similar results have been obtained in all cases.

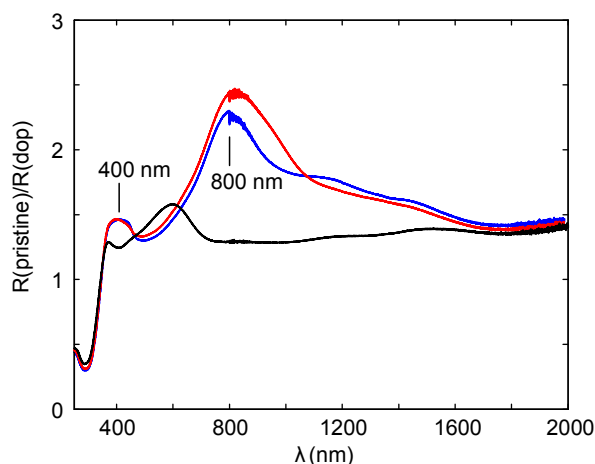


**Figure 12.** UV-Vis reflectance spectra N-sADPA (67 wt% ADPA vs Nylon 6) electrospun nanofibers:  $t_{OX} = 150\text{ s}$  (black);  $t_{DOP} = 60\text{ s}$  (red);  $t_{DOP} = 60\text{ s}$  after 1 h (blue).  $R(\text{pristine})/R(\text{doped})$  spectra.

In the UV-Vis spectra (fig. 12), the band at  $620\text{ nm}$  characteristic of PANI emeraldine base disappears with HCl doping, while two bands at ca.  $800\text{ nm}$ , and  $400\text{ nm}$  were found, the latter being ascribed to a convolution of the two bands at ca.  $360\text{ nm}$  and at  $440\text{ nm}$  which are related to the  $\pi\text{-}\pi^*$  and polaron- $\pi^*$  transitions, respectively<sup>68</sup> (as recorded spectra are reported in ESI Figure 8). The band at lower energy (e.g.  $800\text{ nm}$ ) is related to  $\pi$ -polaron transition. For sake of clarity, the energy diagram for PANI-ES is reported, in figure 10. Interestingly, the doped material evolved with time and, in the spectrum collected one hour later, some bands slightly arise in the region of  $1000\text{-}1500\text{ nm}$ , whose appearance may be ascribed to the relaxation along the chain structure of polarons and bipolarons.

The modifications of the IR spectra induced by doping involve different vibrational modes, indeed, it is expected that a large portion of the spectrum changes upon doping as the size of the

polaron and bipolaron is large thus involving several chemical units; within this frequency range, many weak, medium, and sometimes very strong bands may be observed. A school of thought<sup>69</sup> claims that the doping induced infrared spectrum is only the result of a “spreading” of the electronic intensity on the infrared spectra. The phenomenon is called “Fano resonance” and is still under study for simple systems.

Samples were analyzed right after the doping step, once the membranes were dried. The collected spectra of the protonated samples are reported in figure 13.

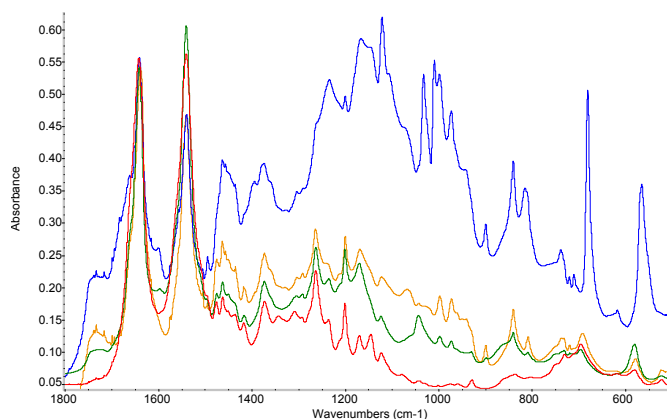


**Figure 13** FTIR spectra in wavenumbers range  $1800\text{-}500\text{ cm}^{-1}$  before doping (red) and after doping:  $t_{DOP} = 30\text{ s}$  in  $\text{H}_2\text{SO}_4$  0.175 M (green);  $t_{DOP} = 30\text{ s}$  in HCl 0.175 M (orange);  $t_{DOP} = 30\text{ s}$  in p-TSA 0.175 M (blue).

Looking at the range of the spectrum from ca.  $1400$  to ca.  $900\text{ cm}^{-1}$  as arising from the vibrations of polarons or bipolarons, HCl and  $\text{H}_2\text{SO}_4$  reveal to be a weak doping agents because band intensities related to the protonated emeraldine salt do significant increase. Protonation still remains not efficient even if the dopant concentration increases.

Conversely, p-TSA turned out to be a more efficient doping agent than HCl or  $\text{H}_2\text{SO}_4$  as IR spectrum shows a strong doping-induced increase in intensity.

Incidentally, for systems where the counterion has featuring chemical structure, its own normal modes may be recognized with a few characteristic bands which do originate from motions localized right in the counterion. These particular features can be well observed in the case of p-TSA: the hydrogen sulfonate counterion of tosylate may be evidenced by the band at  $1040\text{ cm}^{-1}$  that is attributed to the symmetric  $\text{SO}_3$  stretching. New bands appear at  $900\text{ cm}^{-1}$  and  $560\text{ cm}^{-1}$  by doping and both are due to  $\text{SO}_3^{3-}$  group of p-TSA<sup>29</sup>.

## Conclusions

Homogenous and defect-free emeraldine salt PANI nanofibrous membranes consisting in Nylon 6 core and polyaniline (PANI) sheath were demonstrated by means of electrospinning combined with template polymerization. Although the general procedure could consist in the introduction of an oxidant salt that promotes the polymerization in the feed solution to be electrospun, this strategy turned out to be not successful even in the case of the segregation of  $\text{FeCl}_3 \cdot 6\text{H}_2\text{O}$  onto the fibers surface. Nevertheless, segregation was exploited in the new two-step process herein proposed where N-phenyl-1,4-phenylenediamine (ADPA) is loaded into the Nylon 6 feed solution and then polymerized upon immersion of the composite fibers into a solution containing an oxidant and an

acidic species. The control over the process resulted excellent, providing homogenous fibers of ca.  $140 \pm 20$  nm which maintained the same morphology during the polymerization step. Formation of PANI sheath onto the fibers surface was demonstrated by monitoring the polymerization by UV-Vis and FTIR spectroscopy. The composite Nylon 6/PANI nanofibrous membranes were doped to give the emeraldine salt. Among the different acids, the most effective doping has been obtained with p-TSA.

The method herein proposed provides an easy, simple, rapid method for the production of remarkable free-standing emeraldine salt PANI membranes which, combining the high surface to volume ratio of the electrospun mats with the versatility of polyaniline coating, lead to potential developments in biological applications, chemical sensors and filtration of hazardous elements.

## Acknowledgements

Fondazione Cariplo is acknowledged for financial support through the InDiXi project grant n. 2011–0368.

## Notes and references

<sup>a</sup> Dipartimento di Chimica Materiali e Ingegneria Chimica “G. Natta”, Politecnico di Milano, piazza Leonardo da Vinci 32, 20133 Milano, Italy

Corresponding Author : Dr. Chiara Bertarelli

e-mail chiara.bertarelli@polimi.it

<sup>b</sup> Istituto Nazionale di Astrofisica, Osservatorio Astronomico di Brera, via E. Bianchi 46, 23807 Merate, Italy

<sup>c</sup> Center for Nano Science and Technology @PoliMi, Istituto Italiano di Tecnologia, Via Pascoli 70/3, 20133 Milano, Italy

Electronic Supplementary Information (ESI) available: [SEM and optical images, UV-vis reflectance spectra, FT-IR spectra and assignment of the main IR bands]. See DOI: 10.1039/b000000x/

1. Z.-M. Huang, Y.-Z. Zhang, M. Kotaki, and S. Ramakrishna, *Compos. Sci. Technol.*, 2003, **63**, 2223–2253.
2. C. P. Grey, S. T. Newton, G. L. Bowlin, T. W. Haas, and D. G. Simpson, *Biomaterials*, 2013, **34**, 4993–5006.
3. Y. Sharma, A. Tiwari, S. Hattori, D. Terada, A. K. Sharma, M. Ramalingam, and H. Kobayashi, *Int. J. Biol. Macromol.*, 2012, **51**, 627–31.
4. Y. Liao, X.-G. Li, E. M. V. Hoek, and R. B. Kaner, *J. Mater. Chem. A*, 2013, **1**, 15390.
5. X.-H. Qin and S.-Y. Wang, *J. Appl. Polym. Sci.*, 2006, **102**, 1285–1290.
6. P. Gibson, H. Schreuder-Gibson, and D. Rivin, *Colloids Surfaces A Physicochem. Eng. Asp.*, 2001, **187-188**, 469–481.
7. H. Fong, W. Liu, C. Wang, and R. A. Vaia, *Polymer (Guildf.)*, 2002, **43**, 775–780.
8. L. Liu, Z.-M. Huang, C. L. He, and X. J. Han, *Mater. Sci. Eng. A*, 2006, **435-436**, 309–317.
9. M. Stasiak, A. Studer, A. Greiner, and J. H. Wendorff, *Chemistry*, 2007, **13**, 6150–6.
10. T. J. Sill and H. a von Recum, *Biomaterials*, 2008, **29**, 1989–2006.
11. J. Pelipenko, P. Kocbek, B. Govedarica, R. Rošic, S. Baumgartner, and J. Kristl, *Eur. J. Pharm. Biopharm.*, 2013, **84**, 401–11.
12. K. S. Rho, L. Jeong, G. Lee, B.-M. Seo, Y. J. Park, S.-D. Hong, S. Roh, J. J. Cho, W. H. Park, and B.-M. Min, *Biomaterials*, 2006, **27**, 1452–61.
13. Y. Zhou, H. Yang, X. Liu, J. Mao, S. Gu, and W. Xu, *Int. J. Biol. Macromol.*, 2013, **53**, 88–92.
14. H. Yoshimoto, Y. M. Shin, H. Terai, and J. P. Vacanti, *Biomaterials*, 2003, **24**, 2077–2082.
15. S. Ramakrishna, K. Fujihara, W. E. Teo, T. C. Lim, and Z. Ma, *An introduction to Electrospinning and Nanofibers*, World Scientific Publishing, 2005.
16. C. J. Luo, S. D. Stoyanov, E. Stride, E. Pelan, and M. Edirisinghe, *Chem. Soc. Rev.*, 2012, **41**, 4708–35.
17. A. Greiner and J. H. Wendorff, *Angew. Chem. Int. Ed. Engl.*, 2007, **46**, 5670–703.
18. W. E. Teo and S. Ramakrishna, *Nanotechnology*, 2006, **17**, R89–R106.
19. J. T. McCann, D. Li, and Y. Xia, *J. Mater. Chem.*, 2005, **15**, 735.
20. X. Wang, C. Drew, S.-H. Lee, K. J. Senecal, J. Kumar, and L. a. Samuelson, *Nano Lett.*, 2002, **2**, 1273–1275.
21. Q. Wang, X. Dong, Z. Pang, Y. Du, X. Xia, Q. Wei, and F. Huang, *Sensors (Basel)*, 2012, **12**, 17046–57.
22. H. Bagheri and A. Aghakhani, *Anal. Chim. Acta*, 2012, **713**, 63–9.
23. H. Dong, U. Megalamane, and W. Jones, in *Abstract Of Papers Of The American Chemical Society*, 2003, vol. 226, p. 1155.
24. H. Bai, L. Zhao, C. Lu, C. Li, and G. Shi, *Polymer (Guildf.)*, 2009, **50**, 3292–3301.
25. A. A. Syed and M. K. Dinesan, *Synth. Met.*, 1990, **36**, 209–215.
26. Z. Chen, C. Dellapina, E. Falletta, M. Lofaro, M. Pasta, M. Rossi, and N. Santo, *J. Catal.*, 2008, **259**, 1–4.
27. H. Wang, L. Ji, D. Li, and J.-Y. Wang, *J. Phys. Chem. B*, 2008, **112**, 2671–7.
28. Y. Xia, J. M. Wiesinger, A. G. Macdiarmid, and A. J. Epstein, *Chem. Mater.*, 1995, **7**, 443–445.

29. R. W. Gumbs, in *Handbook of organic conductive molecules and polymers - vol 2*, ed. H. S. Nalwa, Wiley, Jon, 1997, pp. 505–572.
30. Y. Niu, *Polym. Eng. Sci.*, 2008, **48**, 355–359.
31. M. Jaymand, *Prog. Polym. Sci.*, 2013, **38**, 1287–1306.
32. A. G. Macdiarmid and A. J. Epstein, *Faraday Discuss. Chem. Soc.*, 1989, **88**, 317–332.
33. Q. Lin, Y. Li, and M. Yang, *Sensors Actuators B Chem.*, 2012, **161**, 967–972.
34. I. Sapurina and J. Stejskal, *Polym Int*, 2008, **57**, 1295–1325.
35. L. Zhang, H. Peng, P. a. Kilmartin, C. Soeller, R. Tilley, and J. Travas-Sejdic, *Macromol. Rapid Commun.*, 2008, **29**, 598–603.
36. N. V. Blinova, J. Stejskal, M. Trchová, I. Sapurina, and G. Ćirić-Marjanović, *Polymer (Guildf.)*, 2009, **50**, 50–56.
37. Y. Zhang, Q. Li, L. Sun, R. Tang, and J. Zhai, *J. Hazard. Mater.*, 2010, **175**, 404–9.
38. R. Li, L. Liu, and F. Yang, *Chem. Eng. J.*, 2013, **229**, 460–468.
39. S. Bozkir, M. Sankir, L. Semiz, N. D. Sankir, and A. Usanmaz, 2012.
40. M. Sankir, S. Bozkir, and B. Aran, *Desalination*, 2010, **251**, 131–136.
41. A. Bianco, C. Bertarelli, S. Frisk, J. Rabolt, M. Gallazzi, and G. Zerbi, *Synth. Met.*, 2007, **157**, 276–281.
42. I. D. Norris, M. M. Shaker, F. K. Ko, and A. G. MacDiarmid, *Synth. Met.*, 2000, **114**, 109–114.
43. M. P. Prabhakaran, L. Ghasemi-Mobarakeh, G. Jin, and S. Ramakrishna, *J. Biosci. Bioeng.*, 2011, **112**, 501–7.
44. E. Zampetti, a. Muzyczuk, a. Macagnano, S. Pantalei, S. Scalese, C. Spinella, and a. Bearzotti, *J. Nanoparticle Res.*, 2011, **13**, 6193–6200.
45. M. J. D. León, *Proceeding Natl. Conf. Undergrad. Res.*, 2001, **1**, 1–5.
46. Y. Zhang and G. C. Rutledge, *Macromolecules*, 2012, **45**, 4238–4246.
47. H. Dong, V. Nyame, A. G. MacDiarmid, and W. E. Jones, *J. Polym. Sci. Part B Polym. Phys.*, 2004, **42**, 3934–3942.
48. M. Wei, J. Lee, B. Kang, and J. Mead, *Macromol. Rapid Commun.*, 2005, **26**, 1127–1132.
49. M. Wei, B. Kang, C. Sung, and J. Mead, *Macromol. Mater. Eng.*, 2006, **291**, 1307–1314.
50. K. H. Hong, K. W. Oh, and T. J. Kang, *J. Appl. Polym. Sci.*, 2005, **96**, 983–991.
51. D. Chen, Y. Miao, and T. Liu, *ACS Appl. Mater. Interfaces*, 2013, **5**, 1206–1212.
52. F. Granato, M. Scampicchio, A. Bianco, S. Mannino, C. Bertarelli, and G. Zerbi, *Electroanalysis*, 2008, **20**, 1374–1377.
53. F. Granato, A. Bianco, C. Bertarelli, and G. Zerbi, *Macromol. Rapid Commun.*, 2009, **30**, 453–8.
54. H. Liu, J. Kameoka, D. a. Czaplewski, and H. G. Craighead, *Nano Lett.*, 2004, **4**, 671–675.
55. A. Laforgue and L. Robitaille, *Synth. Met.*, 2008, **158**, 577–584.
56. E. V Canesi, A. Luzio, B. Saglio, A. Bianco, M. Caironi, and C. Bertarelli, *ACS Macro Lett.*, 2012, **1**, 366–369.
57. S. Nair, E. Hsiao, and S. H. Kim, *J. Mater. Chem.*, 2008, **18**, 5155.
58. A. Cho, D. M. Shin, H. W. Jung, J. C. Hyun, J. S. Lee, D. Cho, and Y. L. Joo, *J. Appl. Polym. Sci.*, 2011, **120**, 752–758.
59. H. R. Pant, H. J. Kim, L. R. Bhatt, M. K. Joshi, E. K. Kim, J. I. Kim, A. Abdal-hay, K. S. Hui, and C. S. Kim, *Appl. Surf. Sci.*, 2013, 4–10.
60. A. P. Monkman, D. Bloor, G. C. Stevens, J. C. H. Stevens, and P. Wilson, *Synth. Met.*, 1989, **29**, 277–284.
61. J. Libert, J. Cornil, D. dos Santos, and J. Brédas, *Phys. Rev. B*, 1997, **56**, 8638–8650.
62. R. McCall, J. Ginder, J. Leng, H. Ye, S. Manohar, J. Masters, G. Asturias, A. MacDiarmid, and A. Epstein, *Phys. Rev. B*, 1990, **41**, 5202–5213.
63. N. Gospodinova and L. Terlemezyan, *Prog. Polym. Sci.*, 1998, **23**, 1443–1484.
64. J. Libert, J. Cornil, D. dos Santos, and J. Brédas, *Phys. Rev. B*, 1997, **56**, 8638–8650.
65. A. G. MacDiarmid and A. J. Epstein, *Synth. Met.*, 1994, **65**, 103–116.
66. A. EFTEKHARI, Ed., *Nanostructured Conductive Polymers*, Department of Chemistry, Ohio Institute of Technology, Cleveland, Ohio, USA.
67. G. Ćirić-Marjanović, M. Trchová, E. N. Konyushenko, P. Holler, and J. Stejskal, *J. Phys. Chem. B*, 2008, **112**, 6976–87.
68. W. S. Huang and A. G. MacDiarmid, *Polymer (Guildf.)*, 1993, **34**, 1833–1845.
69. B. Horovitz, R. Österbacka, and Z. V. Vardeny, *Synth. Met.*, 2004, **141**, 179–183.

Journal Name

RSCPublishing

ARTICLE

Polymer Chemistry Accepted Manuscript